Anomalous Electrical Conductivity of Nanoscale Colloidal Suspensions

Suman Chakraborty* and Sourav Padhy

Department of Mechanical Engineering Indian Institute of Technology, Kharagpur-721302, India

ABSTRACT The electrical conductivity of colloidal suspensions containing nanoscale conducting particles is nontrivially related to the particle volume fraction and the electrical double layer thickness. Classical electrochemical models, however, tend to grossly overpredict the pertinent effective electrical conductivity values, as compared to those obtained under experimental conditions. We attempt to address this discrepancy by appealing to the complex interconnection between the aggregation kinetics of the nanoscale particles and the electrodynamics within the double layer. In particular, we model the consequent alterations in the effective electrophoretic mobility values of the suspension by addressing the fundamentals of agglomeration—deagglomeration mechanisms through the pertinent variations in the effective particulate dimensions, solid fractions, as well as the equivalent suspension viscosity. The consequent alterations in the electrical conductivity values provide a substantially improved prediction of the corresponding experimental findings and explain the apparent anomalous behavior predicted by the classical theoretical postulates.

KEYWORDS: nanofluid · electrical conductivity · electrical double layer · agglomeration · colloidal suspension · electrophoretic mobility

Augmented transport properties exhibited by dilute suspensions of nanoscale particles in liquids have triggered intense research investigations over the past few years, primarily motivated by their broad scientific consequences and technological relevance.[1−3] Such particulate suspensions, generically referred to as nanofluids, have often been characterized with substantially higher effective thermal conductivity values as compared to their bulk carrier phases, leading to extremely efficient rates of heat transfer.[4] Stimulating mathematical models have also been developed in this regard, in an effort to benchmark the experimental observations with robust theoretical postulates.[5,6] However, the issue of the effective electrical conductivities of nanofluids has largely been unexplored, particularly in perspective of the advanced electrochemical theories of colloidal suspensions. As such, it has been observed that the electrical conductivity values of nanofluids are substantially overpredicted by the classical models of well-dispersed particulates[5,6] when confronted with benchmark experiments.[7] This discrepancy between theoretical predictions and experimental observations has often been attempted to be abridged with the aid of empirical or semiempirical considerations, with analogies drawn from the thermal conductivity behavior or through the use of equivalent rules of mixtures. Such considerations, however, are not physically complete in nature since the electrohydrodynamic interactions occurring over disparate physical scales within a nanoparticle suspension system are intensely coupled with a number of significant physicochemical criticalities and constraints in a rather complicated and dynamically evolving manner, many of which might appear to be somewhat intuitive in nature but are by no means obvious. A general inference is that, despite its vast scientific and technological importance, electrical conductivity characteristics of nanoparticle suspensions still remain poorly understood. This deficit in theoretical understanding stems from the complexities in describing the underlying interparticle interactions and the associated kinetics (including the Brownian motion and electroconvection) in a detailed, comprehensive, and dynamically evolving manner.

Here what is presented is believed to be a first comprehensive theoretical model for predicting the effective electrical conductivity of nanoparticle suspensions, with adequate experimental validation. In sharp contrast to the standard modeling approaches, the pre-existence of a stable colloidal suspension phase is not presumed *a priori*, but the pertinent morphological and rheological issues are addressed by considering the competing aspects of the dynamically evolving agglomeration−

*Address correspondence to suman@mech.iitkgp.ernet.in.

Received for review June 4, 2008 and accepted September 19, 2008.

Published online September 30, 2008.
10.1021/nn800343h CCC: $40.75

© 2008 American Chemical Society

deagglomeration kinetics. In terms of the electrical conductivity behavior, various facets of aggregation are strongly interconnected and are conflicting in nature. For example, the physical contact of particles in an aggregated network tends to provide a path of high electrical conductivity. In sharp contrast, aggregation effects simultaneously tend to reduce the effective electrical conductivity of the system as compared to that of an equivalent dispersed system with identical solid fractions since the number density of particles in the system gets reduced on account of agglomeration (an aggregate of several particles assumes the behavior of a single particle). In addition, aggregates are characterized with equivalent particulate masses larger than that for individual dispersed particles as well as higher effective viscosities, leading to reduced effective electrophoretic mobilities. Such complex and counteracting interplays of physical events have grossly been overlooked in the classical literature, reporting many of the so-called apparent anomalies. The other important conflict in this regard is the role of the relative electrical double layer (EDL) thickness. Thicker EDLs tend to augment the bulk carrier phase concentration since greater numbers of counterions leave the EDL (Donnan exclusion) in the process. This, in turn, tends to augment the overall electrical conductivity. However, a thicker EDL also results in a reduced electrophoretic mobility, which may consequently tend to reduce the effective electrical conductivity. The resultant effect, nevertheless, is by no means trivial in nature since the aggregation kinetics are also intensely coupled with the pertinent EDL interactions. The present model, in effect, attempts to capture the complex interplay between these strongly inter-related physical mechanisms in a detailed and rigorous manner.

Several distinctive and novel features are introduced into the present model to achieve the above-mentioned feat. First, a fundamental theory is developed to depict the explicit dependence of the aggregation kinetics on the equivalent electrophoretic mobility, through modifications in effective viscosity, solid fraction, and particle size distribution. Second, the agglomeration−deagglomeration kinetics are explicitly linked with the electroconvection and the pertinent EDL interaction mechanisms, exhibiting an implicit dependence of the suspension characteristics on the relative EDL thicknesses (and hence on the electrically conducting behavior of the suspension system). With these fundamental considerations, it is established that the nontrivial characteristics of the electrical conductivity variations of nanoparticle suspensions can be quantitatively captured by the present comprehensive model in a much more improved manner than that achieved by the existing theoretical models, in tune with the pertinent experimental findings.

Fundamental propositions of the present model stem from the fact that the electrophoretic mobility and hence the electrical conductivity of colloidal suspensions may be expressed as a function of the suspension viscosity (η), particle radius (a), and particle volume fraction (ϕ), through a standard equivalent cell model for electrophoretic mobility. The above-mentioned standard model, however, is far from being complete, with regard to its inherent capability in postulating the "effective" values of the parameters η, a, and ϕ, consistent with the underlying agglomeration−deagglomeration mechanisms. In order to incorporate these aspects from fundamental physical considerations, we consider the transience of aggregation kinetics by appealing to the corresponding governing conservation equations. An important physical basis that goes with these considerations is the fact that dynamic interactions between these solid particles lead to the formation of agglomerates. Collisions between the agglomerates may lead to the formation of new agglomerates of larger sizes. At the same time, agglomerates are also likely to break up, giving rise to deagglomerates of smaller sizes. This extent of agglomeration or deagglomeration eventually determines the internal structure of the suspension matrix and its associated rheological characteristics. For example, the agglomerates are likely to entrap some amount of liquid within them. Under localized shear straining effects, the entrapped liquid also tends to behave like a solid, which leads to an enhancement in the effective local solid fraction, beyond the nominal particle fraction value. This modification in the local solid fraction, in turn, leads to a modification in the local effective viscosity, which needs to be fed back into the electrophoretic mobility calculations for obtaining physically consistent predictions. The present approach attempts to establish a fundamental proposition for coupling the agglomerate/deagglomerate evolution morphology with the electrorheological characteristics of the suspension system, instead of resorting to any predefined constitutive relationship with arbitrary fitting parameters.

RESULTS AND DISCUSSION

The theoretical model predictions obtained in this work are comprehensively tested with benchmark experimental data reported in the literature. The experimental protocol details and relevant data are available in Cruz *et al.*[7] In brief, a commercial α-alumina ceramic powder with a measured average particle size of 520 nm was suspended in distilled water (conductivity = 1.0 μS/cm). Samples of all suspensions with variable solid fractions and salt concentrations were centrifuged. Subsequently, measurements of pH and conductivity of all suspensions were carried out.

Figure 1 depicts the variations in the electrical conductivity as a function of the relative EDL thickness for two different solid fraction values. Clearly, a relatively thinner EDL (*i.e.*, higher κavalue) tends to augment the electrophoretic mobility, which in turn enhances the ef-

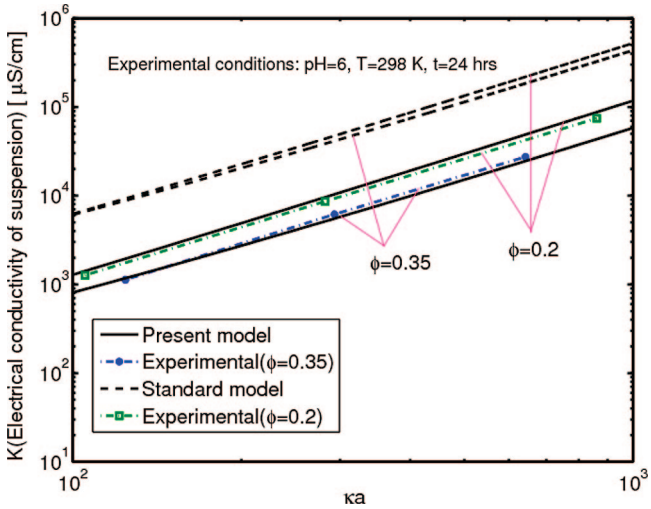

Figure 1. Variation of electrical conductivity with relative EDL thickness. Experimental details and property data corresponding to these results are presented in Cruz *et al.*[7]

fective conductivity. However, these effects are significantly arrested at higher volume fractions since the agglomerated phases formed under such conditions have greater equivalent particulate masses as well as enhanced effective viscosities, leading to reductions in the effective electrophoretic mobility to some extent. These effects, however, are not well captured in the standard theoretical model, as evident from Figure 1. The scenario is particularly interesting if the electrical conductivity ratio, K/K_e, referenced with the conductivity value of the standard solution is plotted as a function of κa, as depicted in Figure 2a. A remarkable agreement between the experimental results and the present theoretical predictions is evidenced from the figure. To derive additional significant physical insight on this matter, Figure 2b is plotted, which depicts the relative conductivity variations with reference to that of the standard solution. As evident from the figure, the standard model tends to predict a monotonically increasing value of the effective conductivity with a thickening of the EDL. This is in accordance with the increasing number of counterions leaving the EDL toward the bulk, following the Donan exclusion principle. However, in reality, this effect is not monotonic in nature. This is because of the counteractive effect that a thicker EDL tends to reduce the effective electrophoretic mobility, which is an effect that is further strongly supported by the formation of agglomerated phases. This results in a reduction in the relative electrical conductivity for substantially thicker EDLs, which is not an effect that is well captured by the standard model.

Figure 3a depicts explicit variations in the electrical conductivity ratio as a function of volume fraction for different solution concentrations. Although the standard model captures the variation more or less in a qualitative manner, the concerned quantitative prediction capability is observed to be quite poor. As such, the standard model is found to substantially overpredict the conductivity ratio, as against the experimental data. This is because of the fact that, while the standard model considers a higher electrical conductivity at higher particle volume fractions because of the greater availability of conducting pathways in the system, it tends to grossly underestimate several critical factors. First, agglomerates are characterized with high mechanical inertia, which makes them behave somewhat sluggishly in a hindered network. Moreover, the strongly dominating attractive interparticle potential in a concentrated system tends to augment the effective viscosity to a considerable extent, leading to a grossly reduced electrical mobility. These effects tend to become progressively severe at higher volume fraction since the agglomeration kinetics dominate more severely over the deagglomeration kinetics. The increasingly more significant deviations between the experimental results and standard theoretical predic-

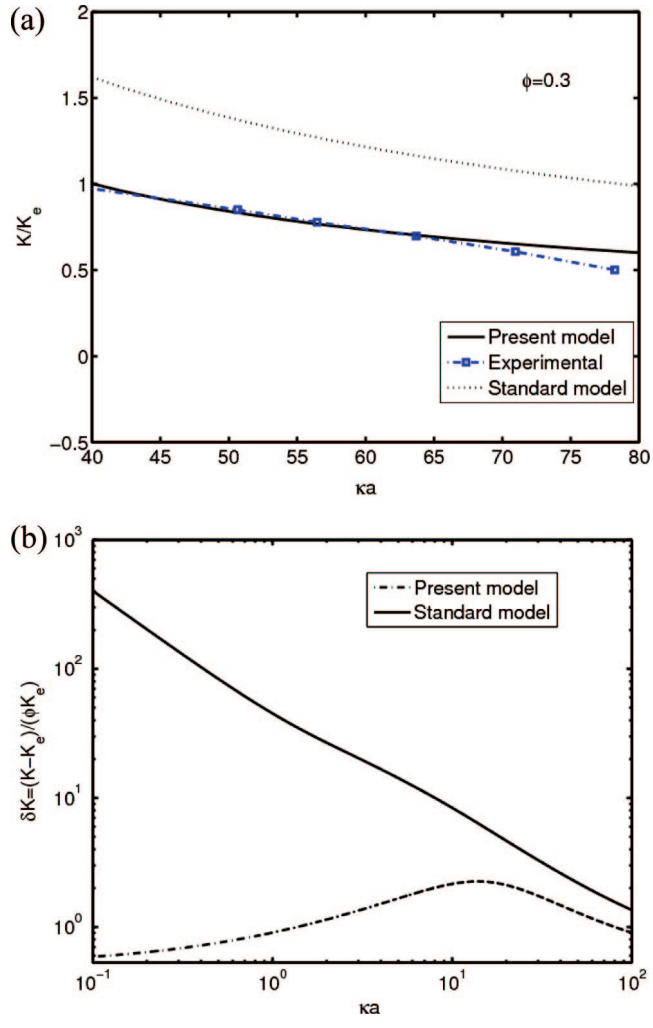

Figure 2. (a) Variation of electrical conductivity with relative EDL thickness, (b) relative deviation between suspension conductivity and solution conductivity values.

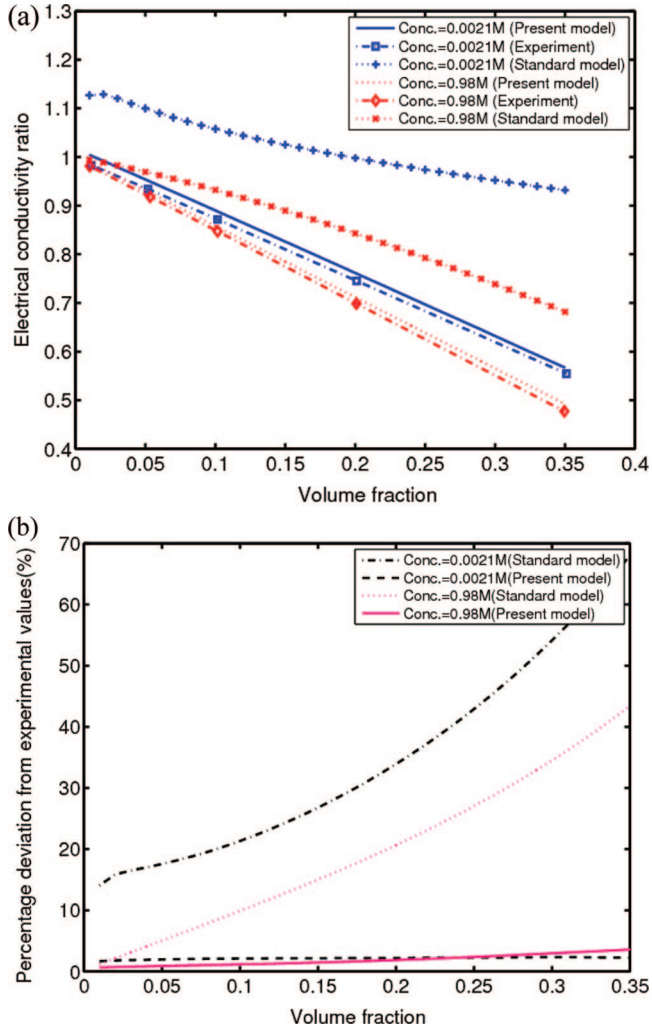

Figure 3. (a) Variation of electrical conductivity with particle volume fraction, (b) percentage deviations of the theoretical predictions from experimental data.

tions are clearly reminiscent of the above phenomenon, as apparent from Figure 3b, which represents the variations in the percentage deviation of the conductivity values from the experimental data, expressed in the following manner: (model prediction − experimental value)/(experimental value) × 100. At lower volume fractions, on the other hand, the agglomeration and deagglomeration kinetics are somewhat more competitive in nature, yielding somewhat less discrepancies between the standard model and the experimental data. The present model, on the other hand, agrees excellently with the experimental data over the entire ranges of nominal concentration and particle volume fraction. Such effects could not be effectively captured through other models reported in the literature.

CONCLUSIONS

We have combined the complex interconnection of electrodynamics within the EDL and the agglomeration−deagglomeration kinetics of the particulate phases with the physics of electro-rheological transport to explain the electrical conductivity behavior of colloidal suspensions. Through this work, we have demonstrated that, apart from the physical properties such as viscosity of liquid, electrical conductivity of liquid, *etc.*, the effective electrical conductivity of colloidal nanosuspensions in a liquid exhibits a complex dependence on the EDL thickness, volume fraction of the suspension, and ionic concentrations, which cannot be effectively captured by the standard mathematical models. The present model, on the other hand, has been designed to be capable of providing accurate quantitative predictions of the pertinent conductivity variations from the fundamental physical principles with minimal empiricism and has been found to quantitatively agree with the experimental trends. The present model, therefore, may act as an important design basis for developing electrically conducting suspension systems under a wide variety of experimental conditions in an effort to optimize the experimental outcome without going through numerous expensive trial runs.

METHODS

For elucidating the present methodology of analysis, one may begin with a brief summary of the fundamental postulates of an equivalent cell model for electrophoretic mobility predictions in a suspension system, in which each particle is considered to be surrounded by a virtual cell such that the particle/solution volume ratio in a unit cell is equal to the particle volume fraction throughout the entire system and the fluid vorticity is zero at the outer surface of the cell. Following this model, we consider spherical colloidal particles of radius a moving with a velocity $\tilde{U}$ in a liquid under an applied electric field $\tilde{E}$. The electrophoretic mobility is defined as $u_p = U/E$, where $U = |\tilde{U}|$ and $E = |\tilde{E}|$. In the cell model, each spherical particle is surrounded by a concentric spherical shell of an adhered fluid phase, having an outer radius of b such that the particle/solution volume ratio in this unit cell is equal to the particle volume fraction ϕ throughout the entire suspension. The origin of the spherical coordinate system (r,θ,φ) is held fixed at the center of one particle. The polar axis $\theta = 0$ is set parallel to $\tilde{E}$. The coupled electrochemical hydrodynamic equations governing the physical behavior of the system are as follows:

$$\nabla \cdot u = 0$$

$$\eta \nabla \times \nabla \times u + \nabla p + \rho_{el} \nabla \psi = 0$$

$$v_i = u - \frac{1}{\lambda_i} \nabla \mu_i$$

$$\nabla (n_i v_i) = 0$$

$$\rho_{el}(r) = \sum_{i=1}^{N} z_i e n_i(r)$$

$$\mu_i(r) = \mu_i^{\infty} + z_i e \psi(r) + kT \ln n_i(r)$$

$$\nabla^2 \psi(r) = \frac{-\rho_{el}(r)}{\epsilon}$$

where $\rho_{el}(r)$ is the charge density, v_i is the velocity of flow of the ionic species, $u(r)$ is the flow velocity of the liquid, λ_i is the drag coefficient, n_i is the number density of the ith ionic species, and z_i is the corresponding valence, μ_i is the electrochemical potential, η is the fluid viscosity, e is the charge of a proton, k is the Boltzmann constant, T is the absolute temperature, ε is the permittivity of the medium, and $\psi(r)$ is the electrical potential. The corresponding boundary conditions are as follows: $u = 0$ at $r = a$; $u = -U \cos\theta$ at $r = b$; $\nabla \times u = \bar{0}$ at $r = b$; $v_i \cdot \hat{n}_i = 0$ (where $\hat{n}_i$ is the unit vector normal to the surface) at $r = a$; $\psi^{(0)} = \zeta$ at $r = a$; $(d\psi^{(0)})/(dr) = (-\sigma)/(\varepsilon)$ at $r \to a^+$; $(d\psi^{(0)})/(dr) = 0$ at $r = b$, where σ is the surface charge density, ζ is the zeta potential, and $\psi^{(0)}$ is the equilibrium potential. The above coupled system of equations yields the following closed-form expression for electrophoretic mobility (with κ as the inverse of the Debye length):[8]

$$u_p = \frac{\varepsilon\zeta}{\eta}\left[\frac{2}{3}\left\{1 + \frac{1}{2(1 + {}^{\delta}/_{\kappa a})^3}\right\}M_1(\kappa a, \varphi) + M_2(\kappa a, \varphi)\right] \quad (1)$$

where

$$M_1(\kappa a, \varphi) = 1 - \frac{3}{(\kappa a)^2}\frac{\varphi}{1-\varphi}(1 + \kappa a Q) + \frac{(\kappa a)^2}{5P}\frac{1}{\varphi^{2/3}}\left(1 + \frac{1-\varphi}{3} - \frac{3}{1-\varphi} + \frac{3\varphi^{1/3}}{1-\varphi}\right) \quad (1a)$$

$$M_2(\kappa a, \varphi) = \frac{2(\kappa a)^2}{9P}\frac{1 + \varphi/2}{1-\varphi}\left(\varphi^{1/3} + \frac{1}{\varphi^{2/3}} - \frac{9}{5\varphi^{1/3}} - \frac{\varphi^{4/3}}{5}\right) \quad (1b)$$

$$P = \cosh[\kappa a(\varphi^{-1/3} - 1)] - \frac{\varphi^{1/3}}{\kappa a}\sinh[\kappa a(\varphi^{-1/3} - 1)] \quad (1c)$$

$$Q = \frac{1 - \kappa a\varphi^{-1/3}\tanh[\kappa a(\varphi^{-1/3} - 1)]}{\tanh[\kappa a(\varphi^{-1/3} - 1)] - \kappa a\varphi^{-1/3}} \quad (1d)$$

$$\delta = \frac{2.5}{1 + 2e^{-\kappa a}} \quad (1e)$$

It is important to mention here that the above model, originally proposed by Oshima, is valid for low zeta potentials and nonoverlapping EDLs in concentrated suspensions, following the Kuwabara cell model and the electrical Levine−Neale (LN) boundary condition. This formalism has subsequently been generalized by introducing Dirichlet type of boundary conditions for the electrical potential instead of the earlier introduced Neumann type of boundary conditions for the cell model. This modification formed the basis of the Shilov−Zharkikh (SZ) model, which was later extended by Cuquejo *et al.*[9] For the LN and SZ models, perturbations to the base state potential ($\psi^{(0)}$), $\delta\psi$, are described in the following distinctive manners, while the pertinent governing differential equations remaining unchanged:

$$(\nabla\delta\psi)\cdot\mathbf{r}|_{r=b} = -E\cos\theta \qquad \frac{dY}{dr}_{r=b} = 1 \qquad \text{LN model} \quad (2a)$$

and

$$\delta\psi|_{r=b} = -Eb\cos\theta \qquad Y|_{r=b} = b \qquad \text{SZ model} \quad (2b)$$

where $\delta\psi = -Y(r)E\cos\theta$. Importantly, the electrical fields consistent with these two models are defined in the following two distinctive manners:

$$\mathbf{E}_{SZ} = -\frac{1}{V}\int_V \nabla\delta\psi dV \quad (3a)$$

$$\mathbf{E}_{LN} = \frac{b}{Y(b)}\mathbf{E}_{SZ} \quad (3b)$$

Because of a further apparent generality of the SZ model in terms of capturing the hydrodynamic interactions between particles for arbitrary volume fractions, we also carry out the electrical conductivity predictions following the route of the SZ model in addition, through the parameters determining the concerned effective electrophoretic mobility values as dictated by the pertinent agglomeration−deagglomeration kinetics. Interestingly, we have observed that, unlike the naïve forms of the SZ and LN models, their adapted versions coupled with agglomeration−deagglomeration considerations virtually yield identical effective electrical conductivity predictions. While this conclusion is too strong to be generalized at this stage on the basis of the limited sets of benchmark experimental data reported in the literature, it may be a subtle implicit indicator of the fact that incorporation of the details of the pertinent agglomeration−deagglomeration kinetics may essentially smooth out the discrepancies in the quantitative predictions from two apparently fundamental models based on distinctive (yet heuristic) choices of boundary conditions. This key feature motivates us toward a further detailing of the agglomeration−deagglomeration mechanisms that lead us to this physically remarkable conjecture.

The mathematical model developed here to represent the aggregation behavior of a suspension of nanoparticles dispersed in a liquid matrix is based on the fundamental proposition that, under the influence of different internal forces, the dynamic interactions between the particles result in the formation of agglomerates and subsequent collisions between agglomerates give rise to new agglomerates of different size distributions. A governing equation for the description of the evolution of number density of the solid particles in the clusters can be described as[10]

$$\frac{\partial}{\partial t}n(r_p, t) = \frac{1}{2}\int_0^{r_p} K(r_p', r_p - r_p')n(r_p', t)n(r_p - r_p', t)dr_p' - n(r_p, t)\int_0^{\infty} K(r_p, r_p')n(r_p', t)dr_p' \quad (4)$$

where $K(r_p, r_p')$ is the agglomeration kernel between the particles of radius r_p and rp', $n(rp', t)drp'$ is the number density of particles with radii between r_p and rp'. In a physical sense, the first integral in the right-hand side of eq 4 represents the creation of particles of radius r_p by agglomeration of particles of radius $rp'(<r_p)$ with particles of radius $r_p - rp'$. The second integral describes the removal rate of particles of by agglomeration with particles of any size. The agglomeration kernel $K(r_p, rp')$ expresses the rate at which particles of radius r_p agglomerate with particles of radius rp'. It needs to be noted here that, in practice, numerical evaluation of the integrals appearing in eq4 may turn out to be rather cumbersome, and discrete summation forms of these expressions can be more conveniently evaluated. The time evolution of agglomerate size distribution, $n_k(t)$, can accordingly be determined by the following rate equation:

$$\frac{\partial n_k(t)}{\partial t} = \frac{1}{2}\sum_{i+j=k} K_{ij}^A n_i(t)n_j(t) - n_k(t)\sum_{i=1}^{\infty} K_{ik}^A n_i(t) \quad (4a)$$

where $n_k(t)$ is the number concentration of agglomerates at time t, composed of k numbers of primary particles. In an aggregation event, agglomerates containing i number of particles attach with agglomerates containing j number of particles to form an aggregate with k ($k = i + j$) number of particles. The agglomeration kernel, Kij, expresses the rate at which agglomerates with i number of particles combines with agglomerates containing j number of particles. Several forms of these kernels have been proposed in the literature to describe the agglomeration mechanism under shear. A standard form of the agglomeration kernel for two colliding particles is proportional to the product of shear rate and the third power of the sum of the collision radii of the two particles, while the

proportionality constant is expressed as a general empirical function of primary particle properties, cluster structure, and fluid flow.[12] In the present model, we consider the Brownian, gravitational, and effective shear interactions (originating out of the resultant van der Waals and the EDL forces) as the basic causualities behind the agglomeration mechanism and develop a fundamental agglomeration model accordingly. Assuming a system of fully destabilized particles with negligible inertia effects, the overall aggregation kernel from these considerations can be written as

$$K_{ij}^{A} = K_{ij}^{BA} + K_{ij}^{GA} + K_{ij}^{SA} \tag{5}$$

The first term in the right-hand side of eq5 corresponds to the agglomeration driven by Brownian motion, in which the interparticle collisions are due to the mutual diffusion of the clusters. The aggregation rate constant in this case is given by[11]

$$K_{ij}^{BA} = \frac{4\pi}{W_{ij}}(D_i + D_j)(R_{c,i} + R_{c,j}) \tag{6}$$

where W_{ij} is a stability ratio which depends on the interactions between colliding aggregates, D_i,D_j are the diffusion coefficients of the particles and are given by the standard Stokes−Einstein relationship. $R_{c,i}$ and $R_{c,j}$ are the collision radii of the two particle clusters and can be given by $\beta_i r_i$ and $\beta_j r_j$, respectively, where β_i is the collision shape factor for ith particle size. In particular,

$$W_{ij} = 1 - \frac{g_{ij}}{r_i + r_j + g_{ij}} + \frac{4(D_i + D_j)}{v_{ij}(r_i + r_j)} \tag{6a}$$

where

$$v_{ij} = \sqrt{v_i^2 + v_j^2}$$

$$v_i = \sqrt{\frac{8k_B T}{\pi m_i}}$$

$$g_{ij} = \sqrt{g_i^2 g_j^2}$$

$$\frac{g_i}{2r_i} = \frac{\left|(2r_i + l_i)^3 - (4r_i^2 + l_i^2)^{3/2}\right|}{3r_i l_i} - 1$$

$$l_i = \frac{8D_i}{\pi v_i}$$

The second term in the aggregation kernel corresponds to the gravitational agglomeration, which occurs as a result of the size dependence of the terminal velocity of small particles. The slowly settling (generally smaller) particles are captured by the more rapidly settling (generally larger) particles, so as to form the gravitational agglomerates. The gravitational agglomeration kernel, K_{ij}^{GA}, can be expressed as

$$K_{ij}^{GA} = \pi(r_i + r_j)^2 \eta_{ij} |\vec{v}_s(r_i) - \vec{v}_s(r_j)| \tag{7}$$

where, $v\rightarrow_s(r)$ is the settling velocity of a particle of radius r, and η_{ij} is the gravitational collision efficiency which is expressed as

$$\eta_{ij} = \frac{y_c^2}{(r_i + r_j)^2} \tag{8}$$

Here, y_c is the critical initial separation between the particles that leads to a grazing contact. Early attempts to estimate this parameter were based on Stokes flow around a sphere moving at its terminal velocity. It was assumed that the presence of the smaller particle had a negligible effect on the flow field around the larger particle. On the basis of these assumptions, Fuchs produced the following analytical expression for the gravitational collision efficiency:[12]

$$\eta_{ij} = \frac{3(r_i / r_j)^2}{2(1 + (r_i / r_j))^2} \tag{9}$$

where $r_j \geq r_i$. When the colliding particles are of similar size, however, $(0.46 \leq (r_i)/(r_j) \leq 1)$, the gravitational collision efficiency is limited to a value of 0.05, which is given by Klett.[13] The third term in the expression for the aggregation kernel represents the effective shear aggregation, the kernel of which can be expressed as

$$K_{ij}^{SA} = \alpha_{ij}^{A} S(R_{c,i} + R_{c,j})^3 \tag{10}$$

where α_{ij}^{A} is the aggregation shape factor and S is the equivalent shear rate. Here we use a collision efficiency model based on the ideas proposed by Kusters *et al.*[14] to express the aggregation shape factor as

$$\frac{\alpha_{ij}^{A}}{\alpha_{max}} = \left[\frac{\exp\left(-x\left(1 - \frac{i}{j}\right)^2\right)}{(i \times j)^y}\right] \tag{11}$$

where i and j indicate the control volume sections where the colliding aggregates are located, α_{max} is a factor (where $0 \leq \alpha_{max} \leq 1$) that denotes the upper value of α_{ij}^{A}. In the present study, we use the parameter values $x = y = 0.1$ and $\alpha_{max} = 1$, following the standard models reported in the literature.[14,15]

It is important to note here that the particle number density distributions described by the above-mentioned agglomeration model may be altered in practice by the deaggregation or break-up mechanisms, which cause the particle clusters to split up into several small fragments. As the aggregates grow, the hydrodynamic stresses may lead to their rupture. This can be accounted for by employing an additional breakage kernel to describe the population of daughter fragments resulting from a breakage event. Modeling of breakage kinetics is still an active area of research and is yet to be understood comprehensively, primarily because of the underlying physical complexities. Two commonly employed variants of the breakage kernel, as reported in the literature,[16] are the corresponding "exponential" and the "power law" forms. Both these models, however, are somewhat empirical in nature and contain too many adjustable parameters to be fitted with experimental constraints. In the present work, we employ a simpler and yet more fundamental approach to model the break-up mechanisms, with an assumption that after the breakup of an aggregate, the resulting fragments are statistically distributed in a uniform manner to all possible smaller size classes, so that the breakage can be modeled as a first-order rate process. This implies that, if a cluster containing N elementary particle breaks, there is an equal chance $1/(N - 1)$ to end up in any size class smaller than N. The rate equation for the breakage kinetics can then be written as

$$\frac{\partial n_k(t)}{\partial t} = \sum_{m=k}^{\infty} \frac{K_m^B n_m(t)}{m} - K_k^B n_k(t) \tag{12}$$

In the process of deaggregation, a cluster of size m is split into a collection of fragments of size k. The corresponding rate constant (breakage kernel) is given by K_m^B. Although breakage can occur by various mechanisms, in most cases, the effect of competing attractive and repulsive forces on the agglomerated particles is considered to be the principle driving mechanisms. With an adequate consideration of the stochastic nature of the strain rate distributions responsible for these interactions, a spatial probability density function, f, can be introduced depicting the probability of having a particular normalized strain rate S/S_{av} at an identified spatial location. Accordingly, one may describe K_m^B as

$$K_m^B = \int_{S_{cr}}^{\infty} SfdS \tag{13}$$

where S_{cr} is a crtitical strain rate for disruption to occur. Physically, the parameter S/S_{cr} is inversely related to the corresponding time-scale ratio t_{cr}/t, where t is the time elapsed during the experimentation and t_{cr} is a limiting aggregation time constant, given by[17]

$$t_{cr} = \frac{\eta \pi r_p^3 W}{kT\varphi} \tag{14}$$

Here W is a stability ratio, given by

$$W = 2r_p \int_0^{\infty} \frac{B(h)}{(h+2r_p)^2} \exp\left(\frac{V_{net}}{kT}\right) dh \tag{15}$$

where V_{net} is the net interaction potential, which is a combined consequence of the van der Waals and EDL forces (for details of expressions of these potentials as functions of the interparticle distance, h, see Russel and Hunter),[18,19] as well as the steric effects represented by the osmostic and elastic potentials. In eq15, $B(h)$ is a factor that takes the hydrodynamic interactions into account and is estimated as[17]

$$B(h) = \frac{6\left(\frac{h}{r_p}\right)^2 + 13\left(\frac{h}{r_p}\right) + 2}{6\left(\frac{h}{r_p}\right)^2 + 4\left(\frac{h}{r_p}\right)} \tag{16}$$

On the basis of these considerations, one may describe the full agglomeration−breakup balance with the following rate equation:

$$\frac{\partial n_k(t)}{\partial t} = \frac{1}{2}\sum_{i+j=k} K_{ij}^A n_i(t) n_j(t) - n_k(t)\sum_{i=1}^{\infty} K_{ik}^A n_i(t) + \sum_{m=k+1}^{\infty} \frac{K_m^B n_m(t)}{m} - \frac{k-1}{k} K_k^B n_k(t) \tag{17}$$

The equilibrium aggregate number density distributions may be calculated by integrating the above equation in time to a steady-state solution. In practice, however, one is usually interested in obtaining the average number of solid particles in a cluster for continuum-based calculations, rather than dealing with the local number density distributions in a cluster. For that purpose, one can define the total number of agglomerates per unit volume in the system at time t, as

$$M(t) = \sum_{i=1}^{\infty} n_i(t) \tag{18}$$

where, $n_i(t)$ is the total number of agglomerates containing i number of particles, per unit volume, in the system at time t. It also follows that the total number of particles per unit volume in the system, N_o, is given by

$$N_o = \sum_{i=1}^{\infty} i n_i(t) \tag{19}$$

One may obtain the average number of solid particles in agglomerates, $n(t)$, as

$$n(t) = \frac{N_o}{M(t)} \tag{20}$$

The effective radius of the aggregates, noting their fractal nature, thus, may be estimated as[17]

$$a = r_p\{n(t)\}^{\frac{1}{d_f}} \tag{21}$$

where d_f is the fractal dimension of the aggregates. Typically, nanofluids are characterized by diffusion-limited cluster−cluster aggregation, for which the concerned weak repulsive barrier implies $d_f \approx 1.8$.

The transient evolution of the agglomeration parameter, $n(t)$, may also be strongly connected with the other morphological and rheological features of the particulate system. In this regard, one of the important implications of the fractal dimension is that it implicitly signifies the degree of roundness, which in turn determines extent to which the liquid molecules may get entrapped into the solid particles. A greater level of entrapment signifies a higher value of effective local solid fraction (since the liquid entrapped within the particle aggregate is forced to move with the same, and hence behaves like an equivalent solid). An effective solid fraction (ϕ'), considering the interparticle network but without taking into account the liquid entrapment, may be estimated from the following expression:[20]

$$\varphi' = C^{\frac{d_f-3}{d_f}} k(3) k(d_f)^{-3/d_f} \varphi^{3/d_f} \tag{22}$$

where ϕ is the nominal solid fraction, C is the number of solid particles per unit volume in the underlying microstructure (which depends on the volume of each atom and the average grain size in the microstructure). For a microstructure with an average grain size of 100 μm, this parameter turns out to be of the order of 10^{16}. The function $k(D)$ in eq 22 may be described as

$$k(d_f) = \frac{\pi^{d_f/2}}{2^{d_f}\left(\frac{d_f}{2}\right)!} \tag{23}$$

With a further consideration of the liquid entrapment within the aggregates, a modified solid fraction may finally be described as

$$\varphi^m = \varphi' + \varphi^{add} \tag{24}$$

where ϕ^{add} is the volume fraction of the entrapped liquid between particle agglomerates, which correlates with the average agglomerate size, $n(t)$. This correlation may be fundamentally postulated by noting that when $\alpha_p = 1$, no liquid is entrapped in the agglomerates, so that

$$\varphi^{add} = \left(1 + \frac{1-\alpha_p}{n}\right)\varphi' \tag{25}$$

The final effective particle fraction is related to the above-mentioned modified volume fraction by relating the same with the effective particle size through the net interaction potential in the following manner:[21]

$$\frac{\varphi^{eff}}{\varphi^m} = \left(\frac{a^{eff}}{a}\right)^3 \tag{26}$$

where

$$a^{eff} = a + \frac{1}{2}\int_{2a}^{\infty}\left[1 - \exp\left(\frac{V_{net}(r)}{kT + K_1 S(r/2)^3}\right)\right]dr$$

and K_1 is a parameter ($K_1 \approx 0.016 + 0.52\phi^m$). The effective viscosity is accordingly calculated as[22]

$$\eta^{eff} = \eta(1 - \varphi^{eff})^{-5/2} \tag{27}$$

With the "effective" parameters determined from the considerations of agglomeration−deagglomeration kinetics described

as above, the equivalent electrophoretic mobility may be conveniently calculated, following eq1. The electrical conductivity of the colloidal suspension, accordingly, may be modeled using the following expression:

$$K = \sum_i c_i u_i q_i \tag{28}$$

where c_i are the number concentrations, u_i are the effective mobilities, and q_i are the electric charges of all the charge carriers present in the system. The corresponding conductivity increment, in relation to that of the carrier phase (K_e), is strongly linked with the ion redistribution in the space occupied by the nanoparticles and their respective EDLs. Following the procedure outlined in Grosse *et al.*,[5] one gets

$$K = \varphi\left\{\frac{3}{4\pi a^3}[4\pi a^2 e(G^+u^+ - G^-u^-) + Q_p u_p] - K_e\right\} + K_e \tag{29}$$

where G^+, G^- are the adsorption coefficients, u^+, u^- are the mobility of the of the ions, Q_p is the charge of the suspended particles, and u_p is the effective mobility of the suspended particles. The expressions for G^+, G^- and Q_p are given by

$$G^{\pm} = 2ac\left[\frac{e^{\mp e\zeta/2kT}-1}{\kappa a} + \frac{2}{\kappa^2 a^2}\tan h\left(\mp\frac{e\zeta}{4kT}\right)\right] \tag{29a}$$

$$Q_p = 4\pi a^2 \frac{2kT\kappa\varepsilon_0\varepsilon}{e}\left[\sin h\left(\frac{e\zeta}{2kT}\right) + \frac{2}{\kappa a}\tan h\left(\frac{e\zeta}{4kT}\right)\right] \tag{29b}$$

where c is the nominal ionic concentration far away from the particle surfaces.

REFERENCES AND NOTES

1. Xie, H.; Wang, J.; Xi, T.; Liu, Y.; Ai, F.; Wu, Q. Thermal Conductivity Enhancement of Suspensions Containing Nanosized Alumina Particles. *J. Appl. Phys.* **2002**, *91*, 4568–4572.
2. Masuda, H.; Ebata, A.; Teramae, K.; Hishinuma, N. Alteration of Thermal Conductivity and Viscosity of Liquid By Dispersing Ultra-Fine Particles. *Netsu Bussei* **1993**, *4*, 227–233.
3. Eastman, J. A.; Choi, S. U. S.; Li, S.; Yu, W.; Thompson, L. J. Anomalously Increased Effective Thermal Conductivities of Ethylene Glycol-Based Nanofluids Containing Copper Nanoparticles. *Appl. Phys. Lett.* **2001**, *78*, 718–720.
4. Hong, T. K; Yang, H-S; Choi, C. J. Study of The Enhanced Thermal Conductivity of Fe Nanofluids. *J. Appl. Phys.* **2005**, *97*, 064311.
5. Grosse, C.; Pedrosa, S.; Shilov, V. N. Corrected Results For The Influence of Size, Æ Potential, And State of Motion of Dispersed Particles on The Conductivity of a Colloidal Suspension. *J. Colloid Interface Sci.* **2003**, *265*, 197–201.
6. Ohshima, H. Electrical Conductivity of a Concentrated Suspension of Spherical Colloidal Particles. *J. Colloid Interface Sci.* **1999**, *212*, 443–448.
7. Cruz, R. C. D; Reinshagen, J.; Oberacker, R.; Segadães, A. M.; Hoffmann, M. J. Electrical Conductivity and Stability of Concentrated Aqueous Alumina Suspensions. *J. Colloid Interface Sci.* **2005**, *286*, 579–588.
8. Ohshima, H. Electrophoretic Mobility of Spherical Colloidal Particles in Concentrated Suspensions. *J. Colloid Interface Sci.* **1997**, *188*, 481–485.
9. Cuquejo, J.; Jiménez, M. L.; Delgado, A. V.; Arroyo, F. J.; Carrique, F. Numerical and Analytical Studies of the Electrical Conductivity of a Concentrated Colloidal Suspension. *J. Phys. Chem. B* **2006**, *110*, 6179–6189.
10. van Dongen, P. G. J.; Ernst, M. H. Kinetics of Reversible Polymerization. *J. Stat. Phys.* **1984**, *37*, 301–324.
11. Elimelech, M.; Gregory, J.; Jia, X.; Williams, R. Particle Deposition & Aggregation In *Measurement, Modelling and Simulation*; Butterworth-Heinemann: Woburn, MA, 1995.
12. Fuchs, N.A. *The Mechanics of Aerosols*; Pergamon: New York, 1964.
13. Klett, J. D.; Davis, M. H. Theoretical Collision Efficiencies of Cloud Droplets at Small Reynolds Numbers. *J. Atmos. Sci.* **1973**, *30*, 107–117.
14. Kusters, K. A.; Wijers, J. G.; Thoenes, D. Aggregation Kinetics of Small Particles in Agitated Vessels. *Chem. Eng. Sci.* **1997**, *52*, 107–121.
15. Selomulya, C; Bushell, G.; Amal, R.; Waite, T. D. Understanding the Role of Restructuring in Flocculation: The Application of a Population Balance Model. *Chem. Eng. Sci.* **2003**, *58*, 327–338.
16. Pandya, J. D.; Spielman, L. A. Floc Breakage in Agitated Suspensions: Effect of Agitation Rate. *Chem. Eng. Sci.* **1983**, *38*, 1983–1992.
17. Prashar, R.; Phelan, P. E.; Bhattacharya, P. Effect of Aggregation Kinetics on the Thermal Conductivity of Nanoscale Colloidal Solutions (Nanofluid). *Nano Lett.* **2006**, *6*, 1529–1534.
18. Russel, W. B.; Saville, D. A.; Schowalter, W. R. *Colloidal Dispersion*;Cambridge University Press: Cambridge, 1988.
19. Hunter, R. J. *Foundation of Colloid Science*; Oxford University Press: New York, 2001.
20. Falconer, K. J. *The Geometry of Fractal Sets*; Cambridge University Press: Cambridge, 1986.
21. Barker, J. A.; Henderson, D. Perturbation Theory and Equation of State For Fluids: The Square-Well Potential. *J. Chem. Phys.* **1967**, *47*, 2856–2861.
22. Ganguly, S.; Chakraborty, S. Stochastic Convective Transport in Presence of Fragmented Dendrites in a Solidifying Binary Melt. *Eur. Phys. J: Appl. Phys.* **2007**, *40*, 221–239.